PROTEINS: Structure, Function, and Genetics 2:308–329 (1987)

Normal Modes of Vibration in Bovine Pancreatic Trypsin Inhibitor and Its Mechanical Property

Tetsuo Nishikawa[1] and Nobuhiro Gō[2]
[1]*Department of Physics, Faculty of Science, Kyushu University, Fukuoka 812;* [2]*Department of Chemistry, Faculty of Science, Kyoto University, Kyoto 606, Japan*

ABSTRACT **The normal mode analysis of conformational fluctuation is carried out for a small globular protein, bovine pancreatic trypsin inhibitor. Results are analyzed mainly to reveal the mechanical construction of the protein molecule. We take dihedral angles, including peptide ω angles, as independent variables for the normal mode analysis. There are 306 such angles in this molecule. Motions in modes with frequencies lower than 120 cm^{-1} are shown to involve atoms in the whole protein molecule, and spatial change of displacement vectors is continuous, i.e., those of atoms near in space are similar. To quantitate the observation of the continuity, a correlation function of direction vectors of atomic displacements is calculated. From this function we define a quantity that is interpreted as the wave length of an equivalent elastic plane wave. From this quantity we deduce effective Young's modulus for each mode. For the mode with the lowest frequency 4.4 cm^{-1}, it turned out to be 0.8×10^9 dyn cm^{-2}, the value two orders of magnitude softer than, for instance, α-helices. Prompted by this observation, the four lowest frequency modes and also the harmonic motions in the thermal equilibrium are analyzed further mainly to detect relatively rigid structural elements in the molecule. From this analysis emerges a mechanical picture of the protein molecule that is made up of relatively rigid elements held together by very soft parts.**

Key words: conformational dynamics, normal mode analysis, Young's modulus, rigid structural elements

INTRODUCTION

Computer simulation approaches have proved powerful to study dynamic aspects of protein conformation. The multitude of complexities of the conformational dynamics, reflected, for instance, in the broad distribution of various characteristic times, requires a set of different computational methods. So far mainly three types of computational methods have been applied successfully to study protein conformational dynamics: 1) molecular dynamics calculation, i.e., numerical integration of the classic Newton equation for positions of atoms in the molecule, 2) normal mode analysis, and 3) Monte Carlo simulation in the space of normal mode variables.

Unlike the normal mode analysis the method of molecular dynamics calculation[1–5] is free from the limitation caused by the assumption of the harmonicity of motion. However, application of this approach is limited to the study of conformational dynamic phenomena occurring in the time range of 10^{-10} s or faster. This is because one step of the numerical integration must be taken in the femto second range so as to be sufficiently shorter than the characteristic time of the fastest conformational motions in protein, i.e., bond stretching vibrations, in order for the integration to be precise.

In the normal mode analysis[6–9] protein conformational dynamics are expressed as a superposition of mutually independent collective motions called normal modes. Underlying this picture of conformational dynamics is a basic assumption of the harmonicity of the energy surface, i.e., the energy surface is assumed to be given by a multidimensional parabola within the range of conformational fluctuations. This assumption is already known to be invalid but is known to be so only in very-low-frequency modes, which are small in number. In a majority of not-very-low-frequency modes the assumption of the harmonicity is valid.[10] The normal mode analysis is useful for understanding dynamics of protein conformation in these modes.

However, a more important usefulness of the analysis exists in providing a natural way of describing or visualizing collective motions in proteins. The collective motions are known to be important in protein function.[11] Functionally important collective motions, which involve necessarily only small amounts of conformational energy change, are expected to be describable as nonlinearly coupled motions of these very-low-frequency normal modes. These normal modes, each of which is a collective motion with a characteristic frequency, can be calculated exactly by an algebraic procedure of the normal mode analysis.

Received August 4, 1987; accepted September 28, 1987.

Address reprint requests to Nobuhiro Gō, Department of Chemistry, Faculty of Science, Kyoto University, Kyoto 606, Japan.

Tetsuo Nishikawa is now at Hitachi Advanced Research Laboratory, Hitachi Ltd, Kokubunji, Tokyo 185, Japan.

The above idea of using the normal mode analysis as a method to define a set of good collective motions for studying highly nonlinear conformational dynamics was realized as the Monte Carlo simulation method with an anisotropic step size.[12] In this method variables corresponding to the normal modes are used as independent variables, and the simulation based on this method was estimated to be more efficient than the molecular dynamics calculation by a factor of 5 to 50 in sampling various conformations from thermally equilibrium ensemble.

To summarize the above, the normal mode analysis is useful to study both harmonic and anharmonic aspects of protein conformational dynamics. Therefore, it is important to know the detailed structure of each of the normal modes. This paper is devoted to characterization of normal modes in a small globular protein, bovine pancreatic trypsin inhibitor (BPTI).

In our previous study of the normal mode analysis of BPTI,[6] we observed the following: 1) In normal modes with frequencies higher than 200 cm^{-1}, motion is localized in one or a few side chains. 2) Normal modes with frequencies in the range of 120–200 cm^{-1} involve motions localized in a few residues, which are adjacent to each other spatially. 3) In modes with frequencies lower than 120 cm^{-1}, motions are not localized but involve most atoms in the whole protein molecule. Moreover, spatial change of displacement vectors is continuous, i.e., those of atoms near in space are similar.

Because of the spatial continuity, displacement vectors in modes of 3 (above) appear as if they were those of a standing wave in a continuous elastic material. This suggests that the protein molecule behaves like an elastic body in such low-frequency modes.

Corresponding to the above observation we give in this paper a quantitative description of localization and spatial continuity of atomic displacement vectors in each normal mode. To describe spatial continuity we calculate space correlation function of direction vectors of atomic displacements. From the correlation function we discuss mechanical properties of the protein molecule regarded as an elastic body. From this analysis emerges an unusually soft image of the protein molecule, which is determined mainly by its very-low-frequency modes. This fact prompted analyses to study the protein from the point of view of its mechanical construction. Because secondary structures are outstanding structural elements in proteins, we pay special attention to their motions in each mode and in thermal equilibrium. Very-low-frequency modes, especially the four lowest frequency modes, are characterized in detail individually.

The picture of protein dynamic structure thus emerging must be supplemented from the anharmonic aspects, which are neglected in the normal mode analysis. We are studying the anharmonic aspects by means of the Monte Carlo simulation.[12] The result of the Monte Carlo simulation will enrich the dynamic picture presented in this paper.

MATERIALS AND METHODS

Choice of Independent Variables for the Analysis

As in the previous paper[6] and also as done by Levitt et al.,[8,9] we take only rotatable dihedral angles as independent variables to carry out the normal mode analysis by fixing bond lengths and bond angles to standard values. The normal mode analysis consists of four main computational steps: 1) minimization of conformational energy starting usually from an X-ray crystallographic structure, 2) calculation of the second derivative matrix of the conformational energy function at the minimum point, 3) calculation of the coefficient matrix for the kinetic energy Lagrangian, and 4) solution of the generalized eigenvalue problem to obtain normal modes. These steps will be explained later. By choosing the dihedral angles as independent variables we can decrease the number of independent variables for the normal mode analysis by a factor of about 8 as compared to the other choice of atomic cartesian coordinates as done by Brooks and Karplus.[7] This factor of about 8 is quite significant for the computational load, especially for steps 1 and 4. In fact the computation of step 1 of the analysis in the cartesian coordinate space by Brooks and Karplus[7] had to be stopped at the point where the second derivative matrix of the conformational energy function still contained seven negative eigenvalues, while in the dihedral angle space we could routinely minimize the conformational energy of small proteins to a point where the gradient virtually vanishes and the second derivative matrix is positive definite.

However, this advantage of the choice of dihedral angles can be enjoyed only after some basic problems concurring with the choice are solved. One of the problems is "regularization" of atomic cartesian coordinates. Because of the choice we must calculate cartesian coordinates of atoms from a set of values of variable dihedral angles by assuming standard values for bond lengths and bond angles. This step of calculation is called generation of conformation. Prior to step 1 mentioned above, we need to calculate a set of dihedral angles that generates an X-ray crystallographic conformation. This is done by regularizing cartesian coordinates so that bond lengths and bond angles have exact standard values. This regularization of coordinates is done by the distance geometry program used previously to calculate conformations from proton-proton distance constraints.[13] The atomic coordinates of BPTI are taken from 4PTI in Protein Data Bank deposited by Huber.[14,15] The regularization is done by treating also peptide ω angles as variables. The root-mean-square displacement (r.m.s.D) of atomic coordinates in the regularized conformation from those in the X-ray conformation is 0.09 Å for backbone atoms.

Minimization of Conformational Energy

By starting from the regularized conformation we minimize conformational energy. As an empirical

conformational energy function we use the UNICEPP energy function developed by Dunfield et al.[16] In this empirical function, hydrogen atoms, which are not involved in hydrogen bond formation, are not treated individually but are treated as absorbed into nonhydrogen atoms, to which they are bonded, to form united atoms. As already mentioned, peptide ω angles are treated as independent variables. In this treatment there are 306 variable backbone and sidechain dihedral angles and 564 atoms.

The energy minimization is done by Newton's method, in the process of which we use both gradient and hessian (second-derivative matrix) of the conformational energy function. This method became a practical one and in fact a very efficient one, because of the recently developed algorithm of rapid calculation of gradient and hessian of conformational energy function.[17,18] The r.m.s.D of backbone atomic coordinates in the energy minimized conformation is 0.92 Å from the X-ray structure.

Mathematical Formulation of the Normal Mode Analysis

Normal mode analysis is a well-established method in molecular physics.[19] Its adaptation to specific problems in proteins has already been described.[9] Here we describe basic mathematical formulation of the normal mode analysis only to the extent necessary to fix the notations and to derive a few specific formulae used in this paper.

We take only dihedral angles as independent variables. In this choice of independent variables the kinetic energy Lagrangian of internal motions in the protein molecule is given by

$$T = (1/2) \sum_{ij} h_{ij} \Delta\dot{\theta}_i \Delta\dot{\theta}_j \tag{1}$$

Note that external motions of the molecule are separated from internal motions in the above expression by the method of Eckart.[20] Therefore, an infinitesimal change $\Delta\theta_i$ of a value of dihedral angle θ_i from the one θ_i^0 at a minimum energy conformation causes infinitesimal changes of atomic coordinates, which are associated only with internal motions. The relation between these two types of infinitesimal quantities are given by the derivatives $\partial \mathbf{r}_a / \partial \theta_i$. Methods of analytical calculation of these derivatives and the coefficients in equation 1 have been described.[21] Matrices whose elements are these derivatives and coefficients are called **K** and **H**, respectively.

The basic assumption of normal mode analysis is that the conformational energy around a minimum is given by a multidimensional parabola, i.e., is given by

$$E = (1/2) \sum_{ij} f_{ij} \Delta\theta_i \Delta\theta_j \tag{2}$$

where the coefficients f_{ij} are the second derivatives of the conformational energy function at the minimum and are calculated by the method developed recently.[17,18] Note that the method of rapid calculation of hessian is used both in the process of minimization and at the minimum point. A matrix whose elements are the second derivatives is called **F**.

The Lagrangian of the system is given by

$$\mathscr{L} = (1/2) \Delta\dot{\theta}^t \mathbf{H} \Delta\dot{\theta} - (1/2) \Delta\theta^t \mathbf{F} \Delta\theta \tag{3}$$

Here $\Delta\theta$ is a vector whose ith component is $\Delta\theta_i$. The superscript t means tranpose. By writing down the Newton equation for the Lagrangian of equation 3, we have

$$\mathbf{H} \Delta\ddot{\theta} + \mathbf{F} \Delta\theta = 0 \tag{4}$$

To solve this equation we express $\Delta\theta$ as linear combination of motions of new (collective) variables $\Delta\sigma$ as follows:

$$\Delta\theta = \mathbf{V} \Delta\sigma \tag{5}$$

where the matrix **V** is such that it transforms the positive definite symmetric matrices **H** and **F** to the identity matrix **I** and a positive definite diagonal matrix Ω, respectively, as follows:

$$\mathbf{H} \rightarrow \mathbf{V}^t \mathbf{H} \mathbf{V} = \mathbf{I} \tag{6}$$

$$\mathbf{F} \rightarrow \mathbf{V}^t \mathbf{F} \mathbf{V} = \Omega \tag{7}$$

In the new collective variables the equation of motion is decomposed into

$$\Delta\ddot{\sigma}_i + (2\pi\nu_i)^2 \Delta\sigma_i = 0 \tag{8}$$

where $(2\pi\nu_i)^2$ is an element of the diagonal matrix Ω. This equation of motion describes a harmonic oscillator, i.e., a normal mode, with frequency ν_i. When one of the collective variables $\Delta\sigma$, say $\Delta\sigma_i$, oscillates with frequency ν_i, the dihedral angles $\Delta\theta$ oscillate with the same frequency and with relative amplitudes given by a vector $\mathbf{v}_i$, which is the ith column vector of matrix **V**. Thus

$$\mathbf{V} = (\mathbf{v}_1, \mathbf{v}_2, \ldots, \mathbf{v}_n) \tag{9}$$

Normalization of the eigenvectors is given by equation 6, i.e.,

$$\mathbf{v}_i^t \mathbf{H} \mathbf{v}_j = \delta_{ij} \tag{10}$$

where δ_{ij} is unity when $i=j$ and vanishes otherwise.

The root-mean-square amplitude of thermal fluctuations of the normal mode variable $\Delta\sigma_i$, which is a harmonic oscillator, is given by

$$(kT)^{1/2}/(2\pi\nu_i) \tag{11}$$

Therefore the root-mean-square thermal amplitude of oscillation of the jth dihedral angle θ_j and ath atom position in the ith normal mode are given, respectively, by

$$v_{ji}(kT)^{1/2}/(2\pi\nu_i) \tag{12}$$

$$D_{ai} = (kT)^{1/2}/(2\pi\nu_i)\sum_j \boldsymbol{k}_{aj}v_{ji} \tag{13}$$

where $\boldsymbol{k}_{aj}$ is an element of matrix **K**, i.e.,

$$\boldsymbol{k}_{aj} = \partial\mathbf{r}_a/\partial\theta_j \tag{14}$$

In the thermally excited ith mode, the displacement vector of ath atom fluctuates along positive and negative directions of vector $\mathbf{D}_{ai}$ with the root-mean-square (r.m.s.) amplitude of D_{ai}. The vector $\mathbf{D}_{ai}$ should be interpreted in this sense as a typical thermal displacement vector of ath atom in ith mode. Interatomic distances also fluctuate in the thermally excited ith normal mode around their mean values at the minimun energy conformation. The change of the distance between a pair of atoms, numbered a and b, is given by

$$\Delta d_{abi} = (D_{ai} - D_{bi}) \cdot (\mathbf{r}_a - \mathbf{r}_b)/|r_a - r_b| \tag{15}$$

for displacement from the mean position by the typical thermal displacement vectors of equation 13. This quantity, signed thermal interatomic distance fluctuation, is either positive or negative depending on the pair, a and b. At a phase of harmonic vibration of ith mode, where atom pairs with positive values of the above quantity are more separated than their mean values, atom pairs with negative values are less separated. The r.m.s. thermal interatomic distance fluctuation is given by the absolute value of the quantity in equation 15.

Localization of Atomic Displacement Vectors in Each Mode

For the purpose of assessing the localization (or nonlocalization) of atomic displacement vectors in each normal mode, we define and calculate the center and the radius of localization in ith normal mode, $\mathbf{L}_i$and R_i, defined as follows:

$$\mathbf{L}_i = \sum_a |\mathbf{D}_{ai}|\mathbf{r}_{a0}/\sum_a |\mathbf{D}_{ai}| \tag{16}$$

$$\mathrm{R}_i^2 = \sum_a |\mathbf{D}_{ai}|(\mathbf{r}_{a0} - \mathbf{L}_i)^2/\sum_a |\mathbf{D}_{ai}| \tag{17}$$

Here $\mathbf{D}_{ai}$ is the r.m.s. displacement vector of ath atom in the ith normal mode given by equation 13. The position vector of ath atom in the minimun energy conformation is denoted by $\mathbf{r}_{a0}$.

Correlation of Directions of Displacement Vectors

As noted in the previous report, atomic motions with frequencies less than 120 cm^{-1} are not localized, and directions of atomic displacements are continuous; i.e., directions of displacements of atoms close in space are similar. In order to make quantitative study of the extent of spatial correlation of directions of displacement vectors in each normal mode, we define and calculate the correlation function of direction vectors of atomic displacements as follows.

For a given normal mode we first focus attention on atoms whose displacement vector is larger in magnitude than 1/20 of the largest displacement vector in the molecule. For such an atom (say, ath atom) we define a direction vector of displacement $\mathbf{A}_i(\mathbf{r}_{a0})$ by $\mathbf{D}_{ai}/|\mathbf{D}_{ai}|$ where $\mathbf{r}_{a0}$ is the position vector of the ath atom in the minimum energy conformation. This direction vector is normalized in the sense that $|\mathbf{A}_i(\mathbf{r}_{a0})| = 1$. Now the correlation function of the direction vector is defined by

$$C_i(d) = \frac{\sum_a\sum_b \mathbf{A}_i(\mathbf{r}_{a0})\mathbf{A}_i(\mathbf{r}_{b0})\,\delta(d - |\mathbf{r}_{a0} - \mathbf{r}_{b0}|)}{\sum_a\sum_b \delta(d - |\mathbf{r}_{a0} - \mathbf{r}_{b0}|)} \tag{18}$$

where δ is the Dirac's delta function, and the summation extends over all atoms for which direction vector $\mathbf{A}_i(\mathbf{r}_{a0})$ is defined. Therefore, the correlation function $\mathrm{C}_i(d)$ is defined as an average of dot products between direction vectors of displacement of a pair of atoms, which are separated in space by distance d.

Fluctuations of Secondary Structures

There are an α-helix and a β-sheet in BPTI, the latter consisting of a pair of anti-parallel β-strands. The normal mode analysis is done in such a way that all external motions of a molecule as a whole are eliminated by the condition of Eckart, and therefore all motions treated are internal. However, when we focus attention on a structural element in the molecule, such as the α-helix, its motion in each normal mode can be divided into two parts, external and internal. The former involves purely translational and rotational motions of a secondary structure, i.e., the part of the fluctuations as a rigid body. The latter is accompanied purely with deformations of the secondary structure. This division is done as follows.

We consider two conformations. One is the minimum energy conformation around which the molecule is fluctuating. The position vector of ath atom in this minimum energy conformation is $\mathbf{r}_{a0}$. The other is an instantaneous fluctuating conformation, in which just the ith normal mode is excited to the r.m.s. thermal amplitude. The position vector of ath atom in this fluctuating conformation is $\mathbf{r}_{a0} + \mathbf{D}_{ai}$. Now we focus attention only on a secondary structure (either

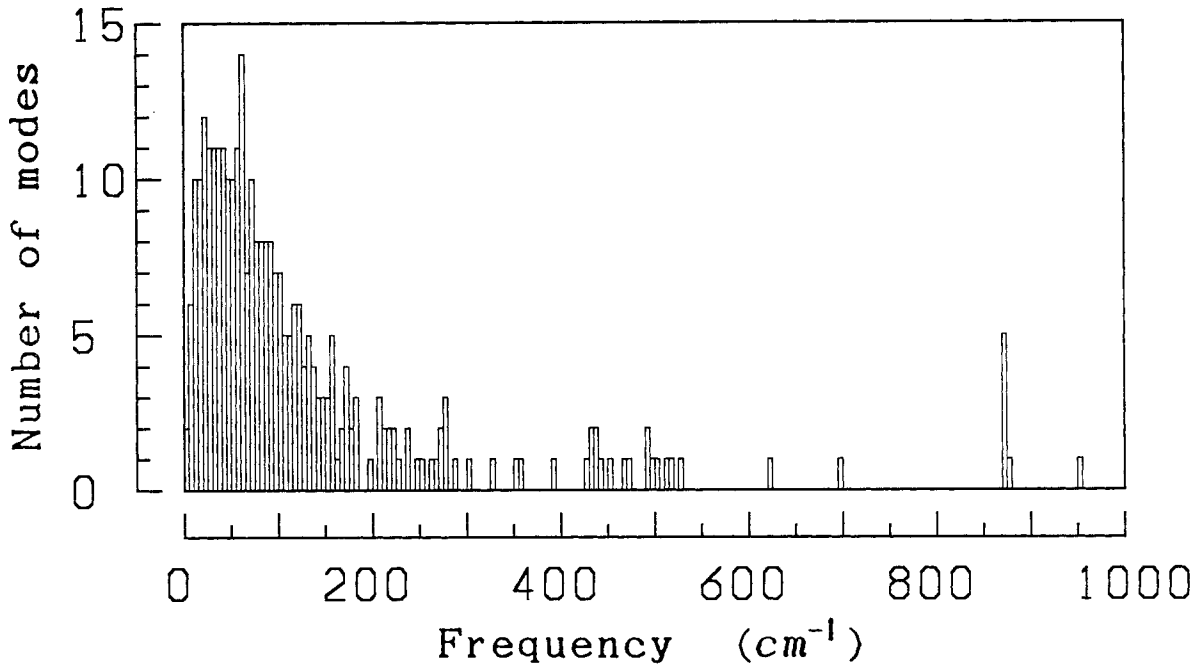

Fig. 1. Histogram of calculated frequencies of normal modes of vibration in a small globular protein, BPTI. The frequencies are shown by corresponding light wave numbers. Number of normal modes in each interval of 5 cm^{-1} is shown.

the α-helix or the β-sheet) in these two conformations, and then bring the secondary structure in the fluctuating conformation purely by translational and rotational motions into the position best fitted with the minimum energy conformation, which gives the least mean square deviations between corresponding main chain atoms. The displacement vector of αth atom after the purely translational and rotational motions will be designated as $\mathbf{D}_{ai}^{e}$. The superscript e stands for "external." The residual displacement vector will be designated as $\mathbf{D}_{ai}^{i}$. The superscript i stands for "internal." The thermal displacement vector of the ith normal mode $\mathbf{D}_{ai}$ is given as a sum of $\mathbf{D}_{ai}^{e} + \mathbf{D}_{ai}^{i}$.

$$\mathbf{D}_{ai} = \mathbf{D}_{ai}^{e} + \mathbf{D}_{ai}^{i} \tag{19}$$

Square deviation in ith mode is then given by

$$\sum_{a}|\mathbf{D}_{ai}|^2 = \sum_{a}|\mathbf{D}_{ai}^{i}|^2 + \sum_{a}|\mathbf{D}_{ai}^{e}|^2 + 2\sum_{a}|\mathbf{D}_{ai}^{i}\cdot\mathbf{D}_{ai}^{e}| \tag{20}$$

The third term on the right-hand side of this equation is found usually to be much smaller than the first two terms. Therefore, the mean-square deviation in the ith mode is decomposed approximately into external (first term) and internal (second term) quantities. Magnitudes of internal and external motions in the each normal mode are defined by dividing the first and second terms by the number of atoms and then taking the square-root of them, respectively.

RESULTS

Frequency Histogram

Distribution of the calculated frequencies is shown in the histogram of Figure 1. Because the number of independent variables in our present treatment is 306, we obtain this number of normal modes and frequencies. The lowest and highest frequencies are 4.4 cm^{-1} and 954.7 cm^{-1}, respectively. There are 254 modes with frequencies below 200 cm^{-1}, which account for 83% of all modes. In the previous calculation,[6] in which we treated the dihedral ω angles around peptide bonds as fixed and used a different conformational energy function, the lowest and highest frequencies were 5.7 cm^{-1} and 665.9 cm^{-1}, respectively. The shift of the lowest frequency toward lower frequency is mainly due to the inclusion of the dihedral ω angles into independent variables. This point was shown as follows. At first all elements pertaining to ω angles are dropped from matrices **F** and **H** obtained in the present calculation. This corresponds to the treatment of fixing these angles at constant values. Then the normal mode analysis is carried out for the remaining submatrices. The frequency of the lowest frequency mode was found to be 5.5 cm^{-1}, which is in very good agreement with the value obtained in the previous calculation. The use of the different empirical energy function appears to have only a small effect on this shift. In the present treatment we allow one extra degree of freedom in the sidechain of arginine residue as compared with the previous treatment. The significantly higher fre-

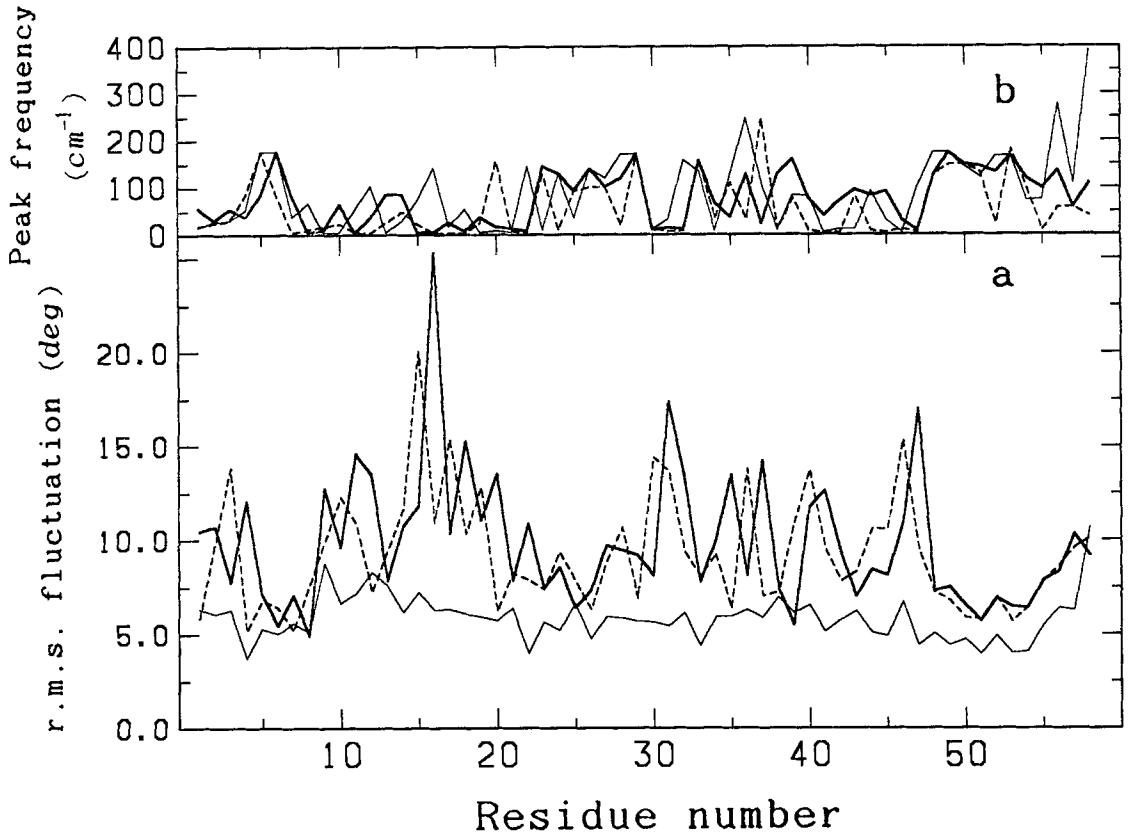

Fig. 2. Site-dependence of fluctuations of dihedral angles. **a:** Root-mean square thermal fluctuations of dihedral angles ω_i, ϕ_i, and ψ_i are plotted against residue number i. **b:** Peak frequency in the fluctuations of the dihedral angles are plotted against residue numbers. Thin solid line, ω; thick solid line, ϕ; broken line, ψ.

quency of the highest frequency mode as compared with the value obtained in the previous calculation is due to a new mode that involves almost exclusively this new extra degree of freedom.

Site-Dependence of Fluctuations of Dihedral Angles and Atom Positions

From equation 12 the mean square of thermal fluctuations of dihedral angle θ_i is given by

$$kT\sum_j (v_{ij}/2\pi\nu_j)^2 \qquad (21)$$

Square root of this quantity for ω_i and for ϕ_i and ψ_i are plotted against residue number in Figure 2a.

The amplitudes of fluctuations of ω_i are rather uniform over residues, and its mean value is 5.8°. Those of ϕ_i and ψ_i differ considerably from site to site. Their mean values are 9.8° and 9.3°, respectively. They are small in the α-helix region (residue 48–56), in the β-turn region (residue 20–30), and in the N-terminal 3_{10} helix region (residue 4–8).

As can be seen in equation 21, fluctuations of dihedral angles are given as sum of contributions from each normal mode. We define the frequency of a normal mode that contributes most to the thermal fluctuations of a certain dihedral angle as its peak frequency. In Figure 2b peak frequencies of backbone dihedral angles are plotted against residue number. The peak frequency ranges from 4.4 cm^{-1} to about 250 cm^{-1}. By comparing Figure 2a and 2b, we see that regions of small fluctuations have high peak frequencies. The residue with the largest angle fluctuations has the smallest peak frequency, 4.4 cm^{-1}.

The above observation suggests that site-dependence of fluctuations of protein backbone are mainly determined by modes with very low frequencies. This was confirmed as follows. The mean square thermal fluctuations of atomic positions is given by a sum of contributions from individual mode $|\mathbf{D}_{ai}|^2$, where $\mathbf{D}_{ai}$ is given by equation 13. Square roots of sums of contributions to r.m.s.D. of C^α atoms from all modes with frequencies below and above a border frequency 30 cm^{-1}, respectively, are plotted in Figure 3. As was noted previously (Fig. 4 in ref. 6), modes with frequencies less than 30 cm^{-1} make major contributions to the thermal fluctuations. We also see that the contributions from modes with frequencies above 30 cm^{-1} do not have clear site-dependence. If we take a frequency lower than 30 cm^{-1} as the border frequency, then site-dependence begins to be observed also in the contributions from modes with frequencies above the border value. Therefore, the site-dependence of r.m.s.D. of C^α atoms is determined mainly by modes

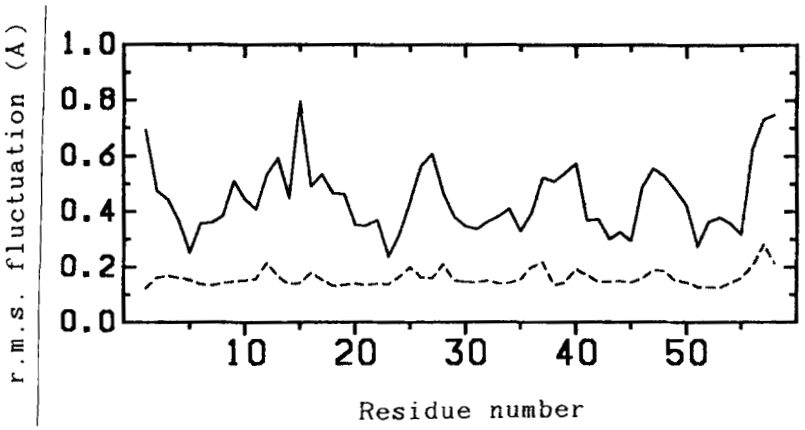

Fig. 3. Site-dependence of fluctuations of positions of C^{α}-atoms plotted against residue number. Solid line, square root of a sum of contributions to mean square fluctuations from modes with frequencies less than 30 cm^{-1}; broken line, same quantity but for contributions from modes with frequencies larger than 30 cm^{-1}.

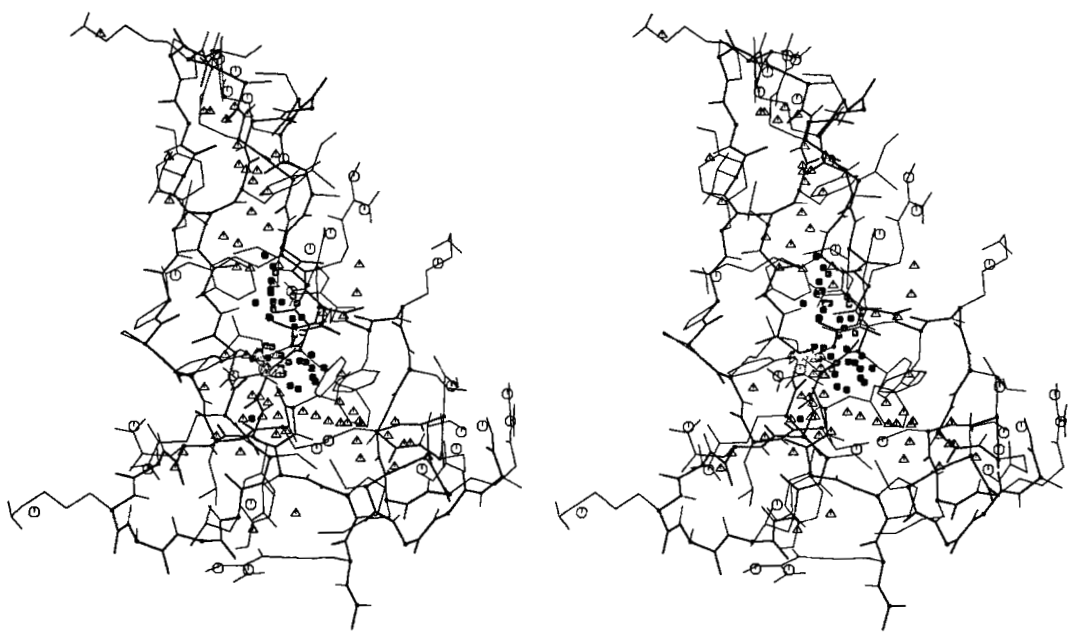

Fig. 4. Stereo drawing of BPTI with centers of localization of normal modes L_i indicated by following symbols: ●, △, and ○ for modes with frequencies in the ranges between 4.4 cm^{-1} and 120 cm^{-1}, between 120 cm^{-1} and 300 cm^{-1}, and above 300 cm^{-1}, respectively. Symbols are given for every five modes for those with frequencies lower than 53 cm^{-1}.

with frequencies below 30 cm^{-1}. Modes with frequencies above 30 cm^{-1} contribute mainly to site-independent "background" motions. Swaminathan et al.[22] have previously made a similar observation by analysis of molecular dynamics trajectory of BPTI. It is interesting that very similar observations are made by the two different methods; the normal mode analysis, which is based on the assumption of the harmonicity of the energy surface, and the molecular dynamics calculation, which is free from the limitation of the harmonicity.

Because biological functions of protein molecules are highly sequence specific in general, we must pay attention to sequence-specific properties in order to understand the mechanism of biological functions. In this respect, modes with frequencies less than 30 cm^{-1}

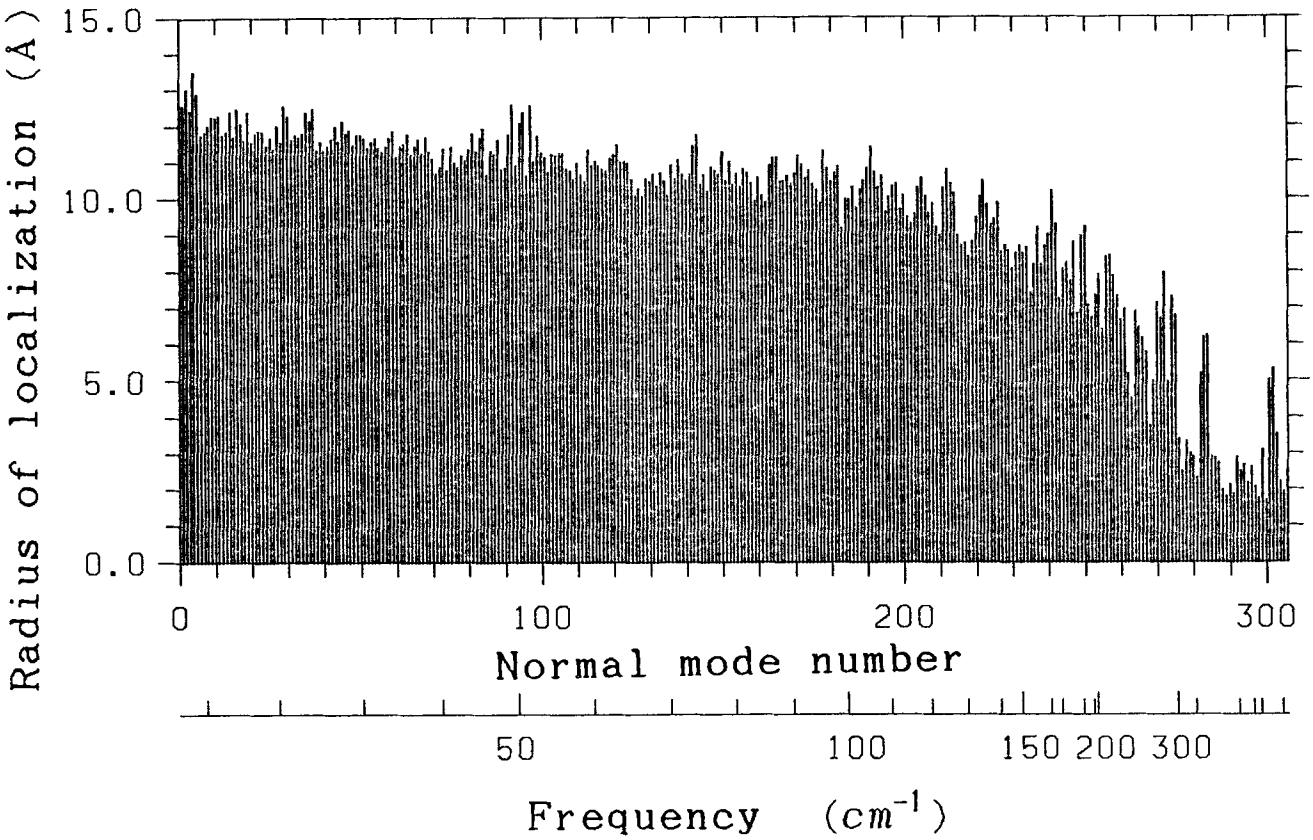

Fig. 5. Radius of localization of normal modes, R_i, is plotted against sequential normal mode number and frequency. The sequential normal mode number is given in the ascending order of frequency.

are expected to be important for biological functions, because mainly they determine the site- and therefore sequence-dependent motions of the molecule.

Figures 2a and 3 can be compared with Figures 4 and 3 in the report by Levitt et al.,[9] respectively, who have done the normal mode analysis of the same protein molecule. The r.m.s. fluctuations of backbone dihedral angles shown in Figure 2a are generally smaller than those calculated by Levitt et al. The site-dependence is appreciably different. However, the r.m.s. fluctuations of positions of C^{α} atoms, which are essentially shown in Figure 3, are very similar to their results. As is shown in Figure 3, the site-dependence of atomic fluctuations is mainly determined by the normal modes with frequencies less than 30 cm^{-1}. The agreement between the two calculations implies that calculated modes with frequencies less than 30 cm^{-1} are not very sensitive to the choice of the empirical conformational energy functions. However, dihedral angle fluctuations caused by high-frequency modes, which contribute to fluctuations of atomic positions only by site-insensitive small amounts, appear to depend on the choice.

Localization of Atomic Displacement Vectors in Each Mode

Center $\mathbf{L}_i$ and radius R_i of localization of atomic displacement vectors in each normal mode are calculated by equations 16 and 17. In Figures 4 and 5 the calculated results of $\mathbf{L}_i$ and R_i are shown. Stereo drawings of atomic displacement vectors in three modes with high and medium frequencies are shown in Figure 6. From these figures we see the following.

1. In 30 modes with frequencies higher than 300 cm^{-1}, the radii of localization are 2–3 Å, and the sites of localization are located at ends of surface-exposed sidechains. The above values of the radii of localization indicate that only a few atoms at the ends of side chains are involved in these modes. Stereo drawing of atomic displacement vectors in a mode with frequency of 492.1 cm^{-1} is given in Figure 6a.

2. In 68 modes with frequencies between 120 cm^{-1} and 300 cm^{-1}, the radii of localization are 3–10 Å, and the sites of localization are located within one or two residues from the surface of the molecule. The above values of the radii of localization indicate that

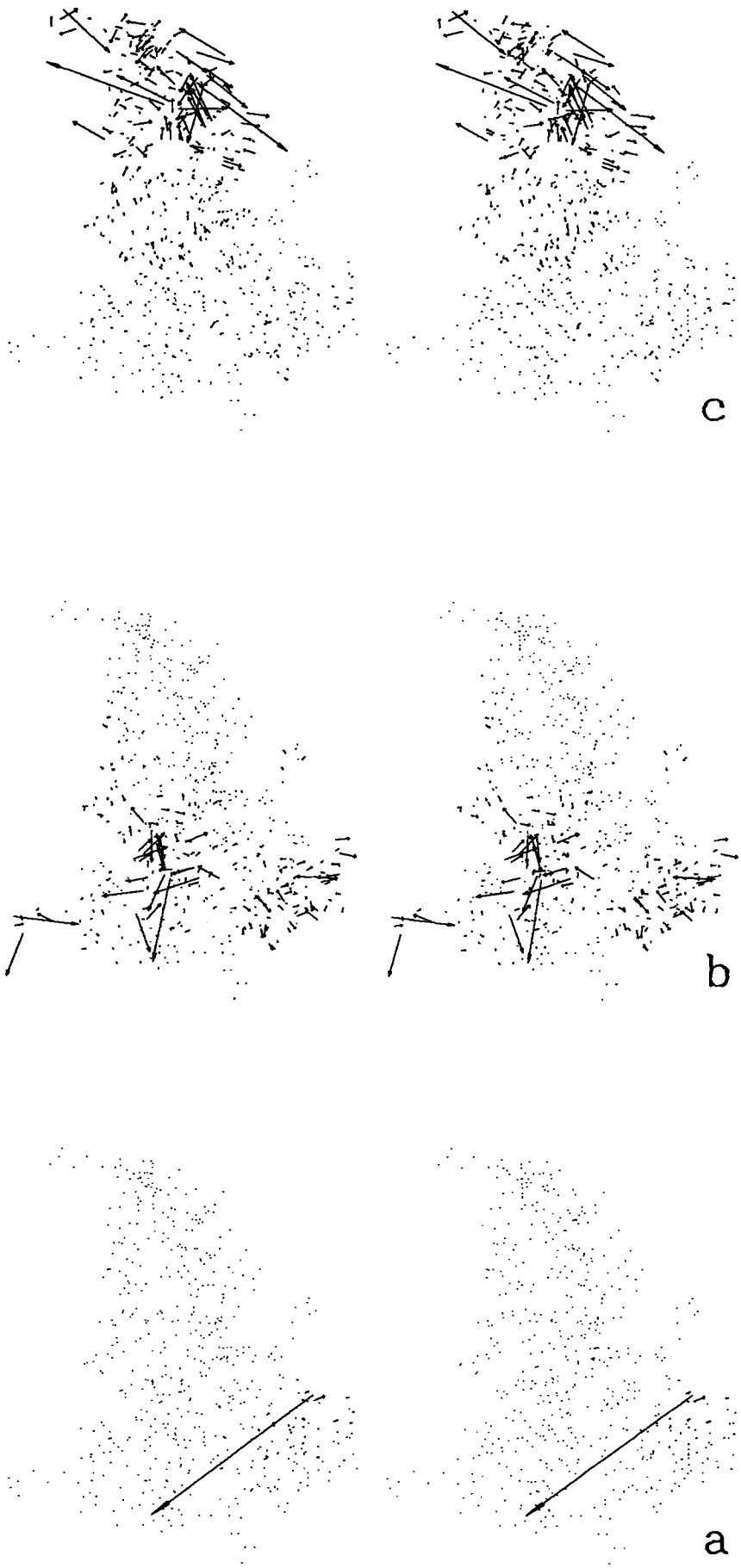

Fig. 6. Stereo drawing of atomic displacement vectors in modes with frequency 492.1 cm^{-1}, 176.7 cm^{-1}, and 128.3 cm^{-1} are shown in a, b, and c, respectively. The molecule is in the same view as in Figure 4. Lengths of the displacement vectors are magnified 100 times of the r.m.s. thermal amplitude at 300K for easy perception.

the extent of atomic movements ranges from those involving a few residues to those involving the whole molecule. Stereo drawing of atomic displacement vectors in two modes with frequencies 176.7 cm^{-1} and 128.3 cm^{-1} are shown in Figure 6b and c, respectively. In Figure 6b atomic displacement vectors are localized in two sites, one around residue 5 and the other around residue 55. Motions in these two sites may be coupled by the S–S bridge between cys 5 and cys 55.

3. In 208 modes with frequencies less than 120 cm^{-1} the radii of localization are mostly in the range of 10–13 Å and the sites of localization are centered in the middle of the molecule. These values of radii indicate that the whole molecule is involved in the motion of each mode.

The site-dependence of the thermal fluctuations was found in Figure 3 to be determined mainly by modes with frequencies less than 30 cm^{-1}. It is interesting that high-frequency modes, which tend to be localized, contribute to the site-independent background motions, and very-low-frequency modes, which are nonlocalized, mainly determine the site-dependence.

Correlation of Directions of Displacement Vectors

In order to make quantitative assessment of spatial correlation of directions of displacement vectors, correlation function of the direction vectors is calculated according to equation 18. Calculated correlation functions are shown in Figure 7a–c for three normal modes with frequencies 11.7 cm^{-1}, 37.2 cm^{-1}, and 92.0 cm^{-1}. In all three curves $C_i(d)$ decreases monotonically from unity to vanish at certain values d_1. As d becomes larger than d_1, $C_i(d)$ becomes negative and then again vanishes at certain values d_2, which are about twice d_1. In the mode with frequency 11.7 cm^{-1} $C_i(d)$ again becomes positive for d larger than d_2. In the other two modes $C_i(d)$ stays small for d larger than d_2. The rough behaviors of the curves for d larger than about 30 Å are due to statistical fluctuations. The correlation functions $C_i(d)$ for modes with frequencies 4.4–30 cm^{-1} have similiar appearance with that for mode with frequency 11.7 cm^{-1}. The curves for modes with frequencies 30–120 cm^{-1} are similar to those for modes with frequencies 37.2 cm^{-1} and 92.0 cm^{-1}.

For understanding the significance of the above features of correlation function, we now discuss $C_i(d)$ for a model system. Protein molecules are expected to behave like a continuous body in their low-frequency modes. As an idealized model of low-frequency mode in a continuous medium, we consider a plane (longitudinal or transverse) wave in the infinite three-dimensional space. Simple calculation shows that

$$C_P(d) = (-1)^{k+1}\,[k(k+1)\lambda/(2d) + 2d/\lambda - (2k+1)] \qquad (22)$$

where the subscript P stands for plane wave, λ is the wavelength of the plane wave, and k is $[2d/\lambda]$—i.e., the integral part of $2d/\lambda$. Figure 7d shows this curve for λ = 20 Å. This curve vanishes when d is an integral multiple of $\lambda/2$. We see that $C_P(d)$ and $C_i(d)$ are very similar for $d < d_2$. From this similarity it is suggested that d_1 in $C_i(d)$ may be interpreted as the average internodal-plane distance.

Figure 7a–c appears to indicate that the values of d_1 become smaller when the frequencies become larger. In order to see this point, d_1 is calculated for all modes with frequencies 4.4–120 cm^{-1}. The calculated result is shown in Figure 8. As expected, d_1 decreases from 6 Å to 11 Å for modes with frequencies 4.4–30 cm^{-1} to 3.5–4.0 Å for modes with frequencies 60–120 cm^{-1}.

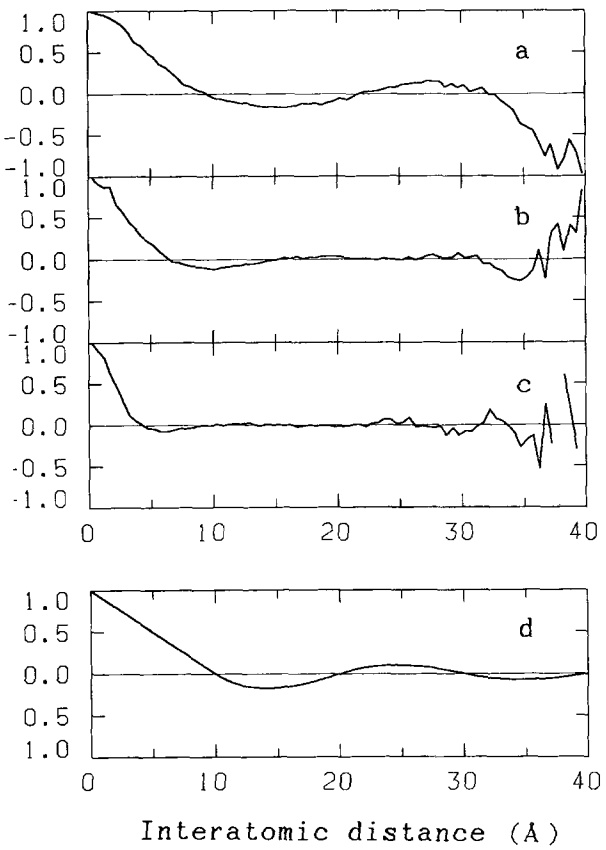

Fig. 7. Correlation function of direction vectors of atomic displacements calculated for three normal modes with frequencies 11.7 cm^{-1} **(a)**, 37.2 cm^{-1} **(b)**, and 92.0 cm^{-1} **(c)**. The correlation function is defined by equation 18. In practice, interatomic distance d is divided into sections, each with the length of 0.5 Å. Contributions from atom pairs, whose interatomic distance falls into one section, to the correlation function are added up, and the result is regarded as the value of the correlation function at the central value of the section of the interatomic distance. The same function calculated for a plane wave with wavelength of 20 Å is shown in **d**.

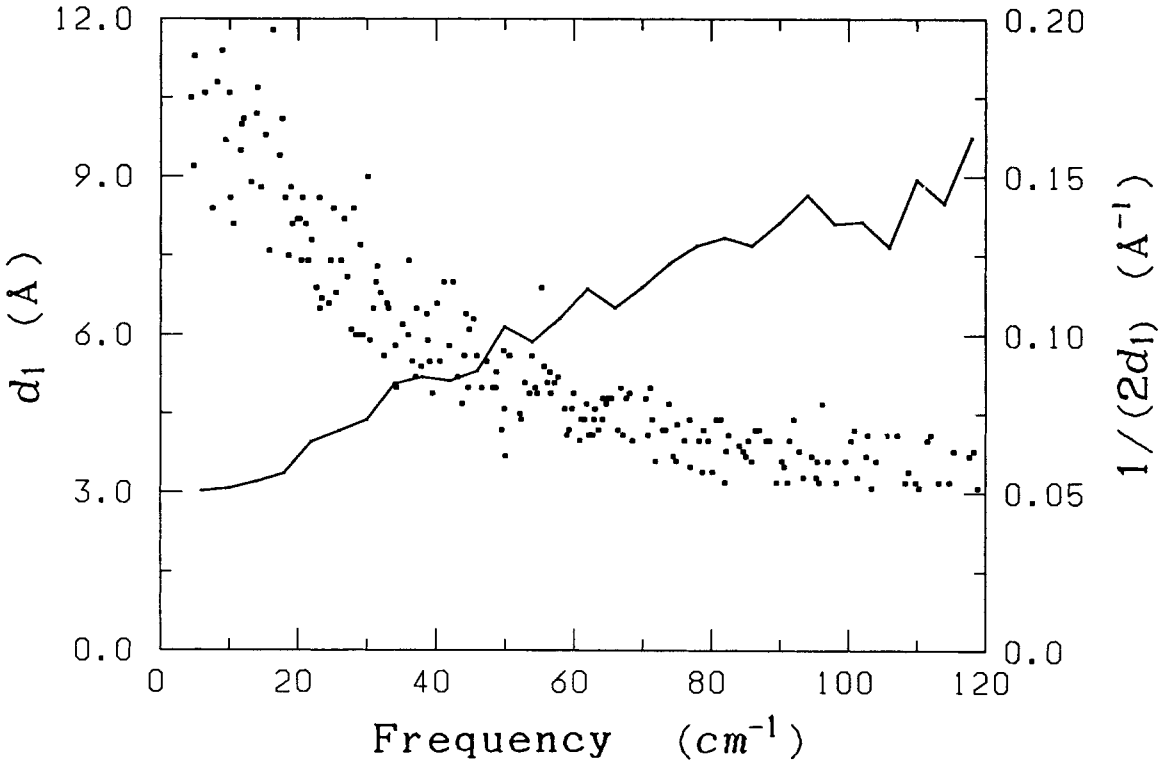

Fig. 8. Value of d_1, the smallest interatomic distance at which the correlation function $C_i(d)$ for the ith mode vanishes, is plotted against the frequency of the mode as a dot. The values of d_1 of modes with frequencies falling in each range of 4 cm^{-1} interval are averaged, and then $1/(2d_1)$ is plotted against frequencies as a thick curve.

TABLE I. Effective Mechanical Properties of BPTI in Very-Low-Frequency Normal Modes

	Normal mode			
Frequency of normal mode in wave No. k of corresponding light in cm^{-1}	4.4	30	60	120
Internodal-plane distance d_1 in Å	10.6	6.8	4.5	3.3
Velocity v (= $2ckd_1$) of equivalent plane wave in 10^2 m s^{-1}*	2.8	12	16	24
Young's modulus E in 10^{11} dyn cm^{-2}	0.008	0.14	0.27	0.6

*c is the light velocity, i.e., $c = 3.0 \times 10^8$ m s^{-1}

Stereo drawings of atomic displacements in the three modes with frequencies 11.7 cm^{-1}, 37.2 cm^{-1}, and 92.0 cm^{-1} are shown in Figure 9a–c. Figure 9c is a typical example of modes with frequencies 60–120 cm^{-1}. The values of d_1 in these modes (3.5–4.0 Å) coincide with sum of van der Waals radii of atom pairs in proteins. This fact together with the fact that $C_i(d)$ vanishes for $d > d_2$ indicates that neighboring atoms tend to move in opposite directions, and motions of atom pairs separated more are uncorrelated in these modes. Figure 9b is a typical example of modes with frequencies 30–60 cm^{-1}. The curve of $C_i(d)$ in Figure 7b indicates that neighboring atoms tend to move in the same direction, atom pairs separated by one intervening atom tend to move in opposite directions, and motions of atom pairs separated

Fig. 9. Stereo drawing of atomic displacement vectors in three normal modes with frequencies 11.7 cm^{-1} **(a)**, 37.2 cm^{-1} **(b)**, and 92.0 cm^{-1} **(c)**. The molecule is viewed from the same direction as that in Figure 4. The displacement vectors are magnified by factors of 10, 50, and 100 in a, b, and c, respectively.

more are uncorrelated in these modes. Figure 9a is a typical example of modes with frequencies 4.4–30 cm^{-1}. The curve of $C_i(d)$ in Figure 7a indicates that neighboring atoms tend to move in the same direction, atom pairs separated by one and a half to three and a half intervening atoms tend to move in the opposite direction, and atom pairs separated more tend to move again in the same direction.

By regarding each normal mode as a plane wave and $2d_1$ as its wavelength, $1/(2d_1)$ is plotted against frequency (expressed in the wave number of the corresponding light) in Figure 8. Slope of a line connecting a point on this curve and the origin of the graph gives a reciprocal of the velocity of the plane wave. The velocity derived in this way is given in Table I for four typical frequencies.

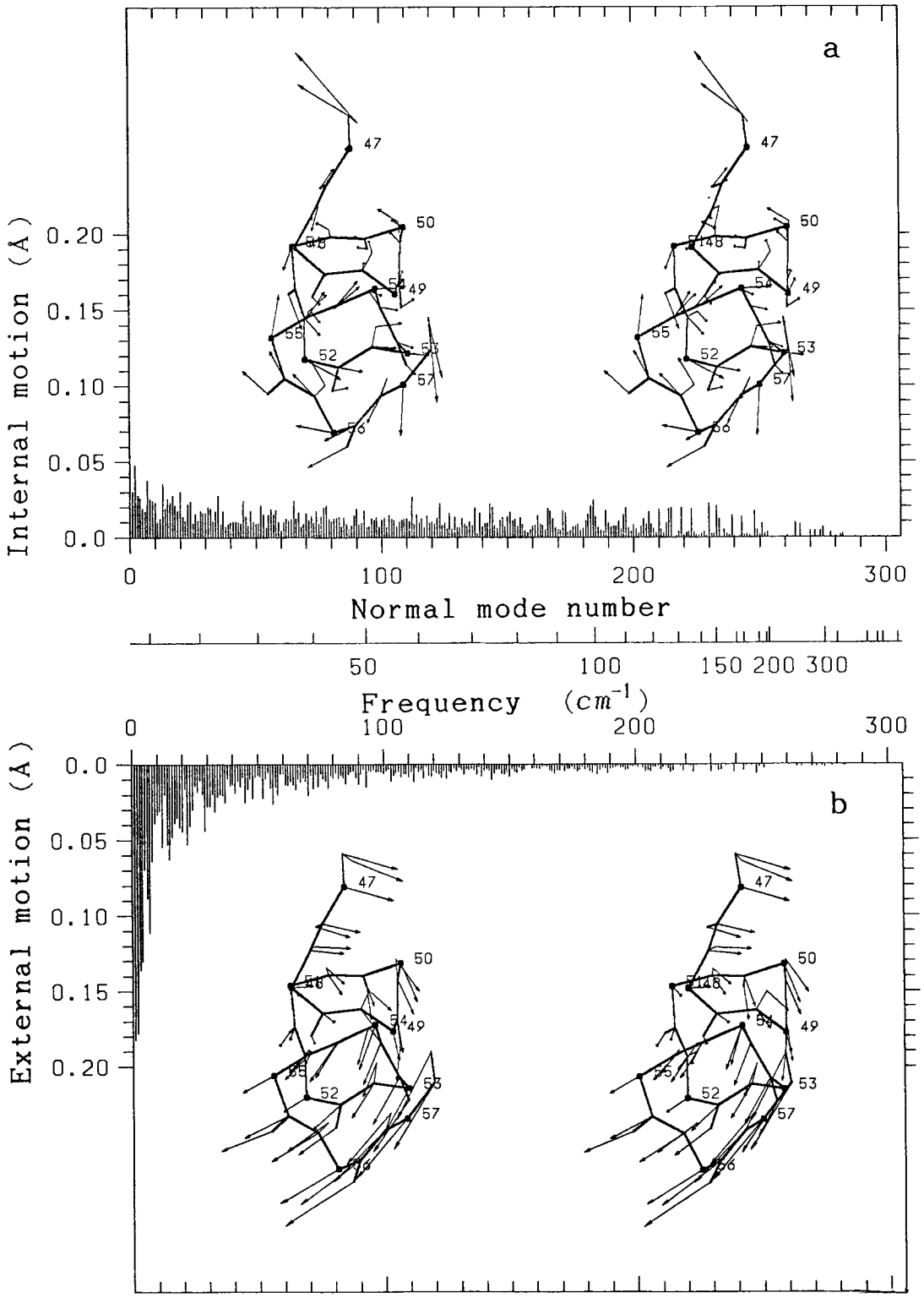

Fig. 10. Magnitudes of internal and external motions of the α-helix in each normal mode are plotted in **a** and **b**, respectively, against the serial normal mode number and frequency. In a, stereo drawing is also shown for internal motions of the α-helix in a normal mode with frequency 5.0 cm^{-1}. The displacement vectors are magnified by a factor of 40. in b, stereodrawing is shown for corresponding external motions in the same mode with a magnification of 10 times.

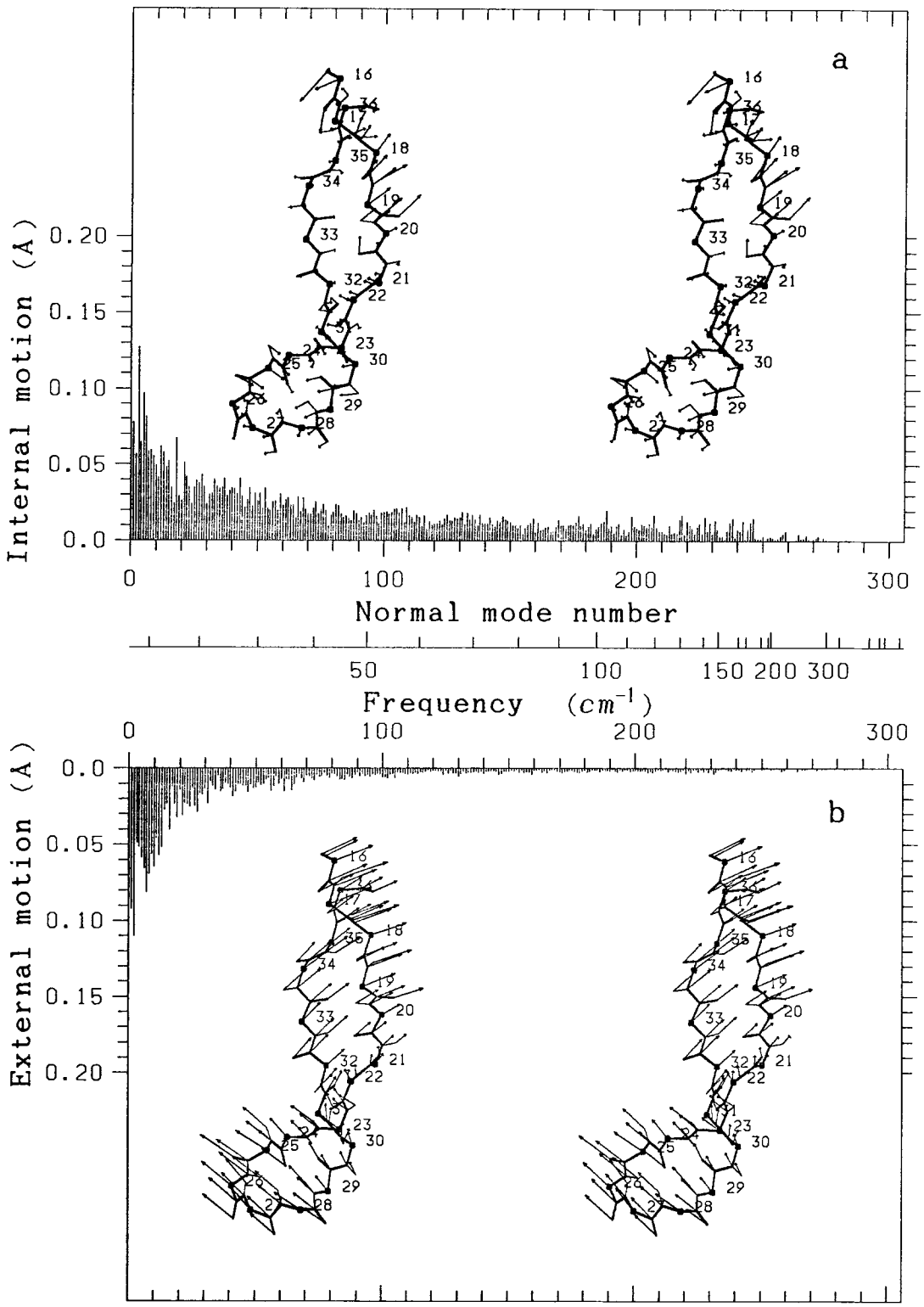

Fig. 11. Magnitudes of internal and external motions of the β-sheet in each normal mode are plotted in **a** and **b**, respectively, against the serial normal mode number or frequency. Stereo drawings of internal and external motions of the β-sheet in a normal mode with frequency 4.8 cm^{-1} are also shown in a and b, respectively. The displacement vectors are magnified by a factor of 20 in both a and b.

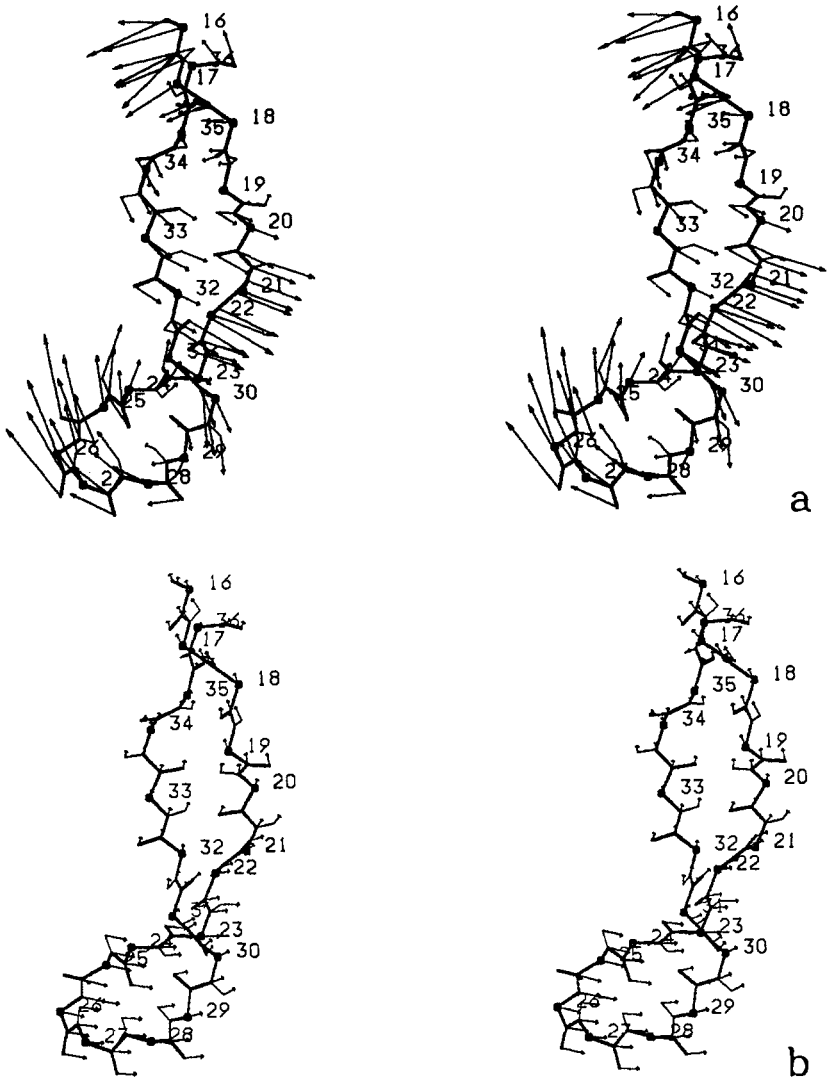

Fig. 12. Stereo drawings of internal and external motions of the β-sheet in a normal mode with frequency 5.0 cm^{-1} are shown in a and b, respectively. Magnification factors are 20.

Velocity of a plane wave in a continuous elastic medium is given roughly by $(E/\rho)^{1/2}$, where E and ρ are Young's modulus and the mass density of the medium. By using this expression and calculated velocities of equivalent plane waves and by assuming 1 g cm^{-1} for the value of ρ, effective values of Young's modulus of the protein molecule in the typical normal modes are estimated and given also in Table I.

Residues 47–57 in this protein form an α-helix. Figure 2b indicates that normal modes with relatively high frequencies make main contributions to the fluctuations of this α-helix. Detailed study indicates that normal modes with frequencies of 100–180 cm^{-1} dominate the fluctuations. This fact together with the fact that the effective value of the Young's modulus for mode with frequency 120 cm^{-1} is 0.6×10^{11} dyn cm^{-2} suggests that the Young's modulus of the α-helix in BPTI is in the range of 10^{11} dyn cm^{-2}. This value agrees well with the one calculated for an isolated α-helix of poly-alanine.[23] The effective value of Young's modulus for the lowest frequency mode with frequency 4.4 cm^{-1} is smaller by about two orders of magnitude. This indicates that the molecule as a whole is much softer than its relatively rigid constituents.

Fluctuations of Secondary Structures

The above finding suggests that mechanical construction of protein molecules may be understood as relatively rigid structural elements held together by softer elements. From such a point of view, motions of secondary structures in each mode are studied.

Residues 47–57 form an α-helix as mentioned before. Residues 16–36 form an antiparallel β-sheet. Motions of these structural elements in each mode are divided into internal and external ones by the method described in the previous section. Their mag-

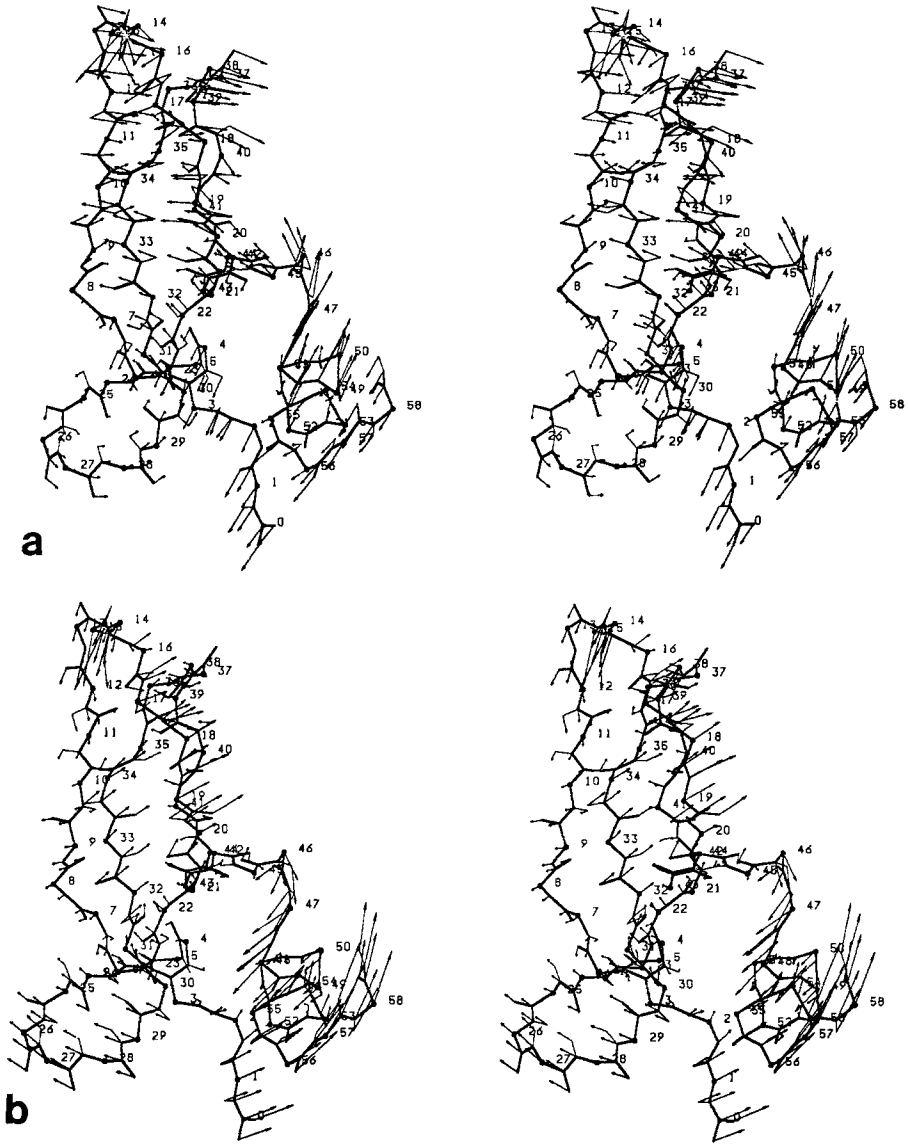

Fig. 13. Stereo drawings of atomic displacements in four lowest-frequency modes with frequencies 4.4 cm^{-1} **(a)**, 4.8 cm^{-1} **(b)**, 5.0 cm^{-1} **(c)**, and 6.4 cm^{-1} **(d)**. The displacement vectors are magnified by a factor of 10.

nitudes in each mode are plotted in Figures 10 and 11 for the α-helix and the β-sheet, respectively.

In Figure 10 we see that the thermal fluctuations in the α-helix are mainly determined by external motions in modes with frequencies lower than 30 cm^{-1}. In modes with frequencies higher than 30 cm^{-1}, internal motions are more pronounced than external motions in the α-helix. In Figure 10 stereo drawings are also shown for internal and external motions of the α-helix in a normal mode with frequency 5.0 cm^{-1}. The internal motion is a twisting motion. Such a twisting motion of the α-helix is often observed in low-frequency normal modes. The external motion is roughly a rotatory motion around cys 51. Comparison between Figure 10a and b clearly shows that external motion dominates in the motion of the α-helix in the normal mode with frequency 5.0 cm^{-1}. In other words, the α-helix behaves relatively rigidly in this mode.

In Figure 11 we see that the thermal fluctuations of the β-sheet in this molecule are mainly determined by internal motions in modes with frequencies higher than 60 cm^{-1}. Both internal and external motions are appreciable generally in modes with frequencies lower than 30 cm^{-1}. Internal and external motions of the β-sheet in two normal modes with frequencies 4.8 cm^{-1} and 5.0 cm^{-1} are shown in Figures 11 and 12, respectively. In the mode with frequency 4.8 cm^{-1} external motion is dominating. In the mode with frequency 5.0 cm^{-1} internal motion is dominating. It is a bending-twisting motion. Two types of motions of the β-sheet exist in the very-low-frequency modes,

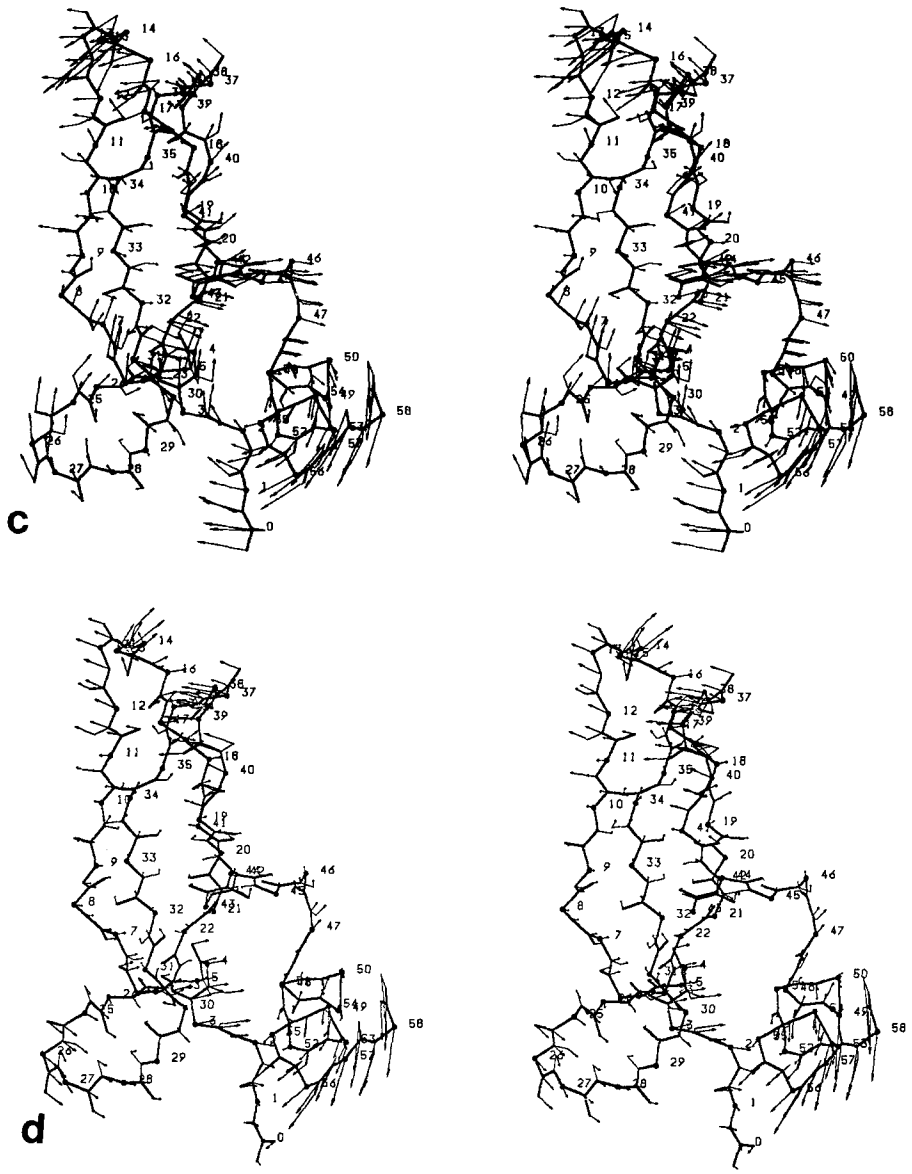

Fig. 13. Continued.

i.e., those with external motions dominating and those with internal motions dominating.

We see that internal fluctuations in the α-helix do not increase appreciably as the frequency of normal mode decreases, while they do so appreciably in the β-sheet. This difference comes from the fact that the β-sheet in this molecule is large as compared to the size of the molecule. In fact it extends over a whole diameter of the molecule. Such a large structure cannot have a large external motion within the molecule because the normal modes are obtained in such a way that there are no external motions in the molecule as a whole.

Very-Low-Frequency Modes

The site-dependence of r.m.s.D of mainchain atoms was found to be determined mainly by modes with frequencies less than 30 cm^{-1} earlier in this section as well as in the previous report.[6] Of these modes, four with frequencies lower than 7 cm^{-1} are studied in detail with respect to their dynamic characteristics. Stereo drawings of atomic displacements in these modes are shown in Figure 13a–d together with the main chain structure. In all of these four modes we can see the spatial continuity of the displacement vectors as noted earlier. We have just seen that the secondary structures, especially the α-helix, behave sometimes as a relatively rigid structural unit in very-low-frequency modes. This finding prompted us to do more systematic analysis to detect relatively rigid structural elements in each of the four modes. This is done by studying relative motions between residues. If relative motions among a certain number of contiguous residues are very small, the segment

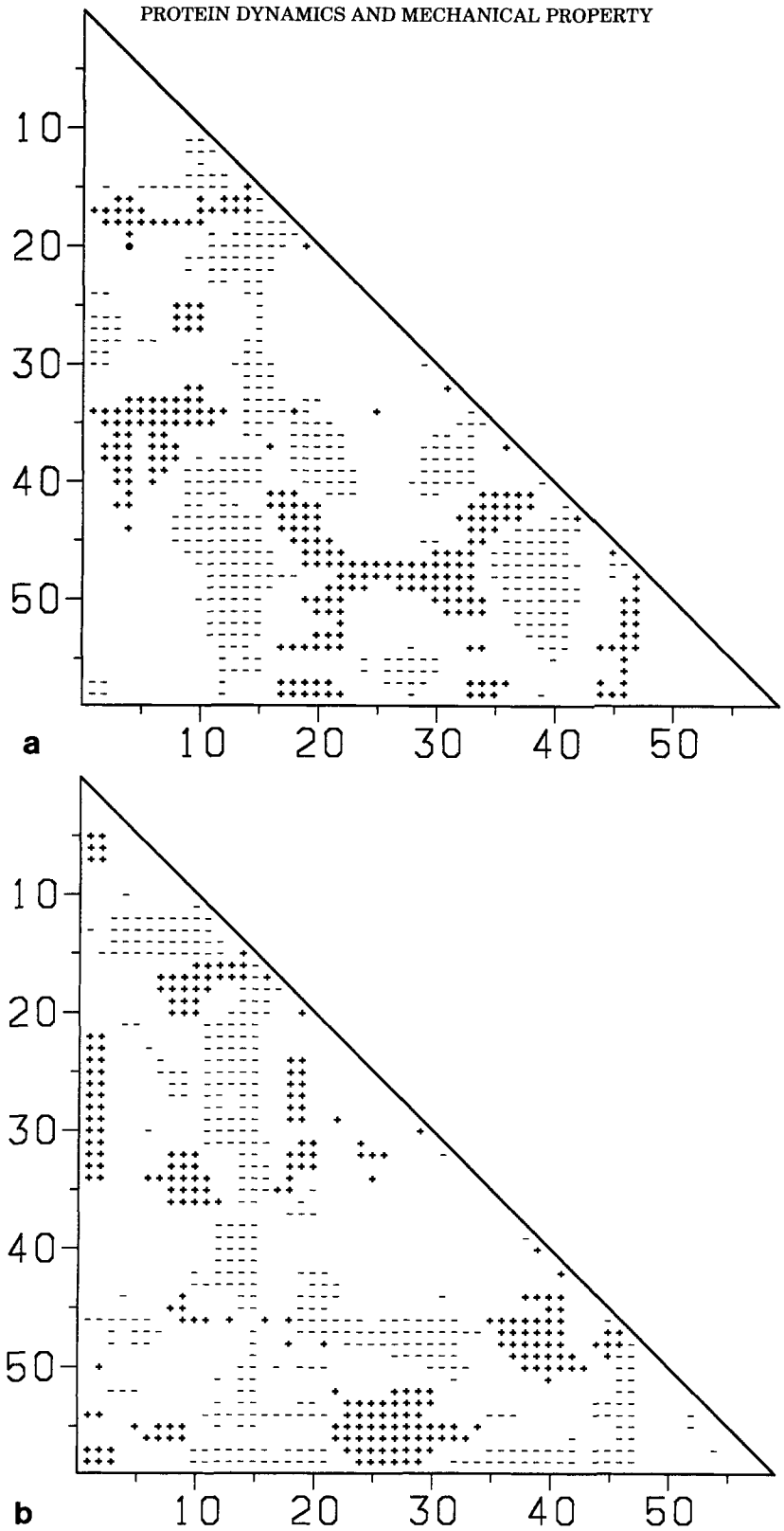

Fig. 14. Maps for distance fluctuations between residues in the same four lowest-frequency modes as in Figure 13. Both ordinate and abscissa are residue numbers. Symbols at a pair of residues indicate relative degrees of fluctuations of distances between them. To calculate them, distance between mth and nth residues is at first defined as the average of distances between main chain atoms belonging to the respective residues. The signed interatomic distance fluctuations between mainchain atoms belonging to these residues are then calculated by equation 15 and averaged. This quantity, D_{mni}, is then normalized by the average of absolute values of $D_{m'n'i}$ over pairs of residues whose interresidue distances fall within the same 1.0 Å interval as that between the mth and nth pair. The normalized quantity N_{mni} is represented at position (n,m) in the triangular map by a symbol + when $N_{mni} > 1$, by a symbol − when $N_{mni} < -1$, and by a blank when $-1 < N_{mni} < 1$. A blank means that distance fluctuations are relatively small. Distance fluctuations between a pair of residues with either + or − are relatively large but with an opposite phase.

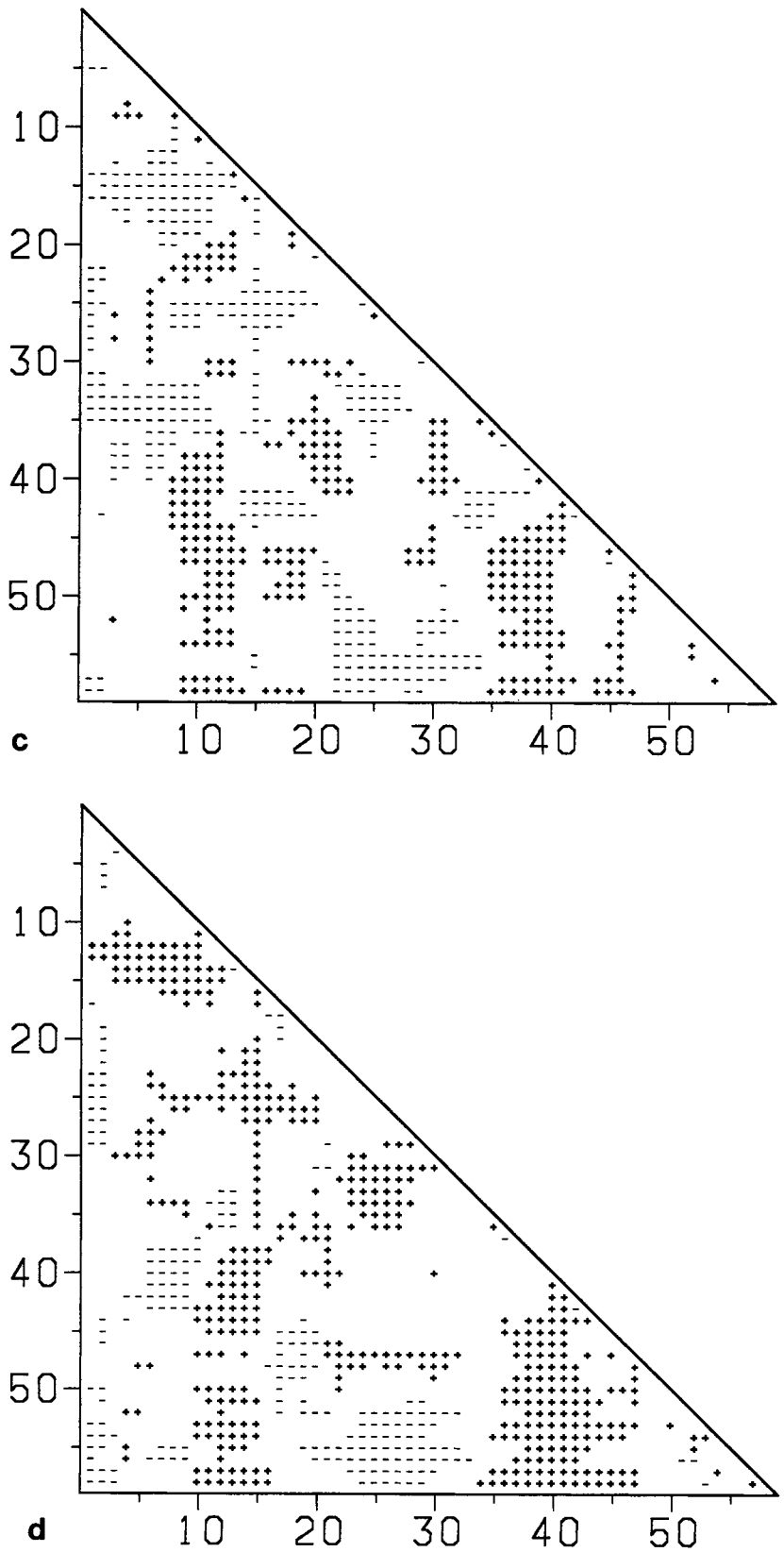

Fig. 14. Continued.

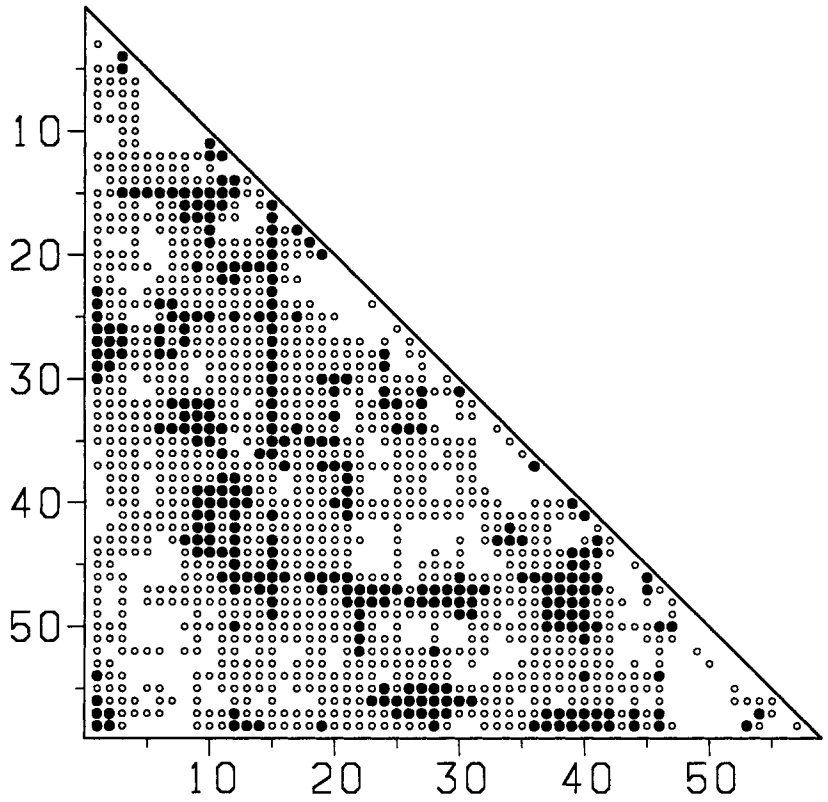

Fig. 15. Relative r.m.s. fluctuations in the thermal equilibrium of distances between atoms belonging to a pair of residues. Both ordinate and abscissa are residue numbers. The r.m.s. fluctuations of a distance between mth and nth residues in the thermal equilibrium is given by the square root of the average of $(D_{mni})^2$ (see Fig. 14) over all normal modes i. This quantity, d_{mn}, is again normalized by an average of the same quantity $d_{m'n'}$ over pairs of residues whose interresidue distances fall within the same 1.0 Å interval as that between the mth and nth pair. The normalized quantity, S_{mn}, is then classified into (a) $S_{mn} > 1.2$, (b) $1.2 > S_{mn} > 0.8$, and (c) $0.8 > S_{mn}$. Those in the classes of a and b are indicated in the map by symbols ● and ○. Those in the class of c are indicated by blanks. From the distribution of the symbols we can identify relatively rigid segments along the chain in the thermal equilibrium.

consisting of such residues is rigid. In order to study relative movements between residues, maps for distance fluctuations between residues are also prepared and are given in Figure 14a–d for the four modes. From patterns of symbols in the triangular maps, we can identify rigid and flexible segments along the chain. A rigid segment along the chain appears as a white triangle on the diagonal. A region near the diagonal corresponding to a flexible segment is filled with symbols. We can also see relative displacements between these segments from the map.

By examination of Figures 13 and 14 for the four modes, we see the following:

Mode with frequency 4.4 cm^{-1}. Four segments along the chain, consisting of residues 1–13, 17–34 (which is the antiparallel β-sheet), 34–40, and 48–58 (which is the α-helix) are rigid. Segments between these rigid ones are flexible. Two rigid segments, 1–13 and 48–58, do not show appreciable relative movements. The N-terminal end of segment 1–13 and the C-terminal end of segment 48–58 are spatially adjacent to each other. They behave dynamically as a unit in this mode. This unit is undergoing a rotatory oscillation about an axis connecting centers of the β-structure and the α-helix. The upper half of the molecule (when viewed from the direction of Fig. 13a) is also undergoing a rotatory oscillation around the vertical axis. Directions of the two rotatory motions are roughly perpendicular.

Mode with frequency 4.8 cm^{-1}. Three segments along the chain, consisting of residues 3–11, 21–43, and 48–58, are rigid. The large central segment contains most of the β-sheet. The last segment consists of the α-helix. The β-sheet and the α-helix are undergoing relative rotatory oscillations about an axis connecting the centers of the two structures. The flexible segment consisting of residues near 46–47 makes this motion possible.

Mode with frequency 5.0 cm^{-1}. Three segments along the chain, consisting of residues 1–7, 42–44, and 48–58 (which is the α-helix), are spatially adjacent to each other and form one dynamically rigid

unit. Other segments show intermediate rigidity. The β-structure undergoes a rather complex oscillation involving both twisting and bending.

Mode with frequency 6.4 cm^{-1}. Three segments along the chain, consisting of residues 5–11, 21–28, and 31–40, are rigid. The central segment consists mainly of the turn at the end of the β-sheet. The α-helix shows an internal motion of a small amplitude.

Detailed description of eight lowest frequency modes calculated by Levitt et al. is given in their paper.[9] We tried to compare each of our four lowest-frequency modes described above with their eight lowest-frequency modes. It was not easy to find a clear correspondence between them. Yet, the combined effects of these respective sets of lowest-frequency modes are quite similar. A parallel experience has been reported in their paper, i.e., when they have carried out the normal mode analysis for two different energy minimum conformations of BPTI, individual lowest-frequency modes are less similar, yet the sums of contributions from them are similar. We also have carried out the same analysis for different energy minimum conformation and have made the same observation.

In order to see the conformational fluctuations in the thermal equilibrium, another triangular map is prepared and is given in Figure 15. From the distribution of the symbols we can identify relatively rigid segments along the chain. They are segments, each consisting of residues 5–11, 19–26 (a part of the β-sheet), 32–39 (also a part of the β-sheet), and 48–55 (the α-helix). The α-helix and a segment consisting of residues 4–7 tend to behave dynamically as a single unit. The disulfide bond between residues 5 and 55 should be responsible for this behavior. From the distribution of the symbols we can identify relatively flexible segments. Segments near residues 15 and 47, respectively, have large root-mean-square distance fluctuations to most of other segments. Large distance fluctuations are observed between two segments, consisting of residues 9–13 and 38–44, between the β-turn and the N-terminus and between the β-turn and C-terminus.

SUMMARY AND DISCUSSION

Analysis in this paper gave quantitative description for the observations made in the previous paper,[6] especially on the collectiveness and spatial continuity of atomic motions in normal modes with frequencies less than 120 cm^{-1}. As a result, a picture of a protein molecule with unusual mechanical softness emerged.

In normal modes with frequencies less than 120 cm^{-1} the whole protein molecule moves collectively and behaves like a continuous body. Such normal modes are therefore similar to a standing wave in a continuous body, which has the same size and shape as the protein and has a certain mechanical property. Such a standing wave may be characterized by disposition of nodal planes. By calculating correlation functions of direction vectors of atomic displacements in a normal mode, a quantity d_1 was defined, which was interpreted as average internodal-plane distance. From this quantity and the frequency of the mode, velocity of equivalent plane elastic wave was estimated. From the estimated velocity, the effective Young's modulus for the mode was deduced. It turned out to be 0.8×10^9 dyn cm^{-2} for the mode with the lowest frequency of 4.4 cm^{-1}.

For the fluctuations of the α-helix near the C-terminus of this protein, normal modes with frequencies in the range of 100–180 cm^{-1} were found to be dominating. Effective Young's modulus for these modes is in the range of 10^{11} dyn cm^{-2}, the same range of values as for isolated α-helices. Other relatively rigid structural elements were also identified. The protein molecule is therefore made up of relatively rigid structural elements held together by very soft parts, making the whole molecule very soft. Collective motions associated with these very soft normal modes are expected to be functionally important. Recently stiffness of crossbridge heads (S1) in single glycerol-extracted muscle fiber was measured to have Young's modulus in the range of 10^9 dyn cm^{-2}.[24]

For the purpose of studying anharmonic aspects of the conformational dynamics, Monte Carlo simulation of conformational fluctuations of BPTI, based on the concept of the collective normal mode variables, has been carried out.[12] Detailed analysis of the results will be reported elsewhere.[25] In this analysis energy minimizations have been carried out by starting from a series of sampled conformations. As a result, a number of different minimum energy conformations are obtained. Thus, the conformational energy surface is far from being harmonic in the sense that there are many minima in the range accessible in the thermal equilibrium. However, this fact does not nullify the significance of the normal mode analysis. The normal mode analyses have been carried out in each of the energy minima obtained by the energy minimization. Comparison of normal modes in each of the energy minima revealed that, even though each individual mode differs from one minimum to another significantly, the conformational subspaces spanned by high- and low-frequency modes, respectively, are rather stable. For example, the subspaces spanned by normal modes with frequencies less than 30 cm^{-1} are about the same for all energy minima. Therefore, the normal mode analysis provides a fairly correct dynamic picture for motions in the orthogonal harmonic subspace, even though anharmonicity is significant in the overall dynamics of the protein structure. Even for motions in the subspace spanned by modes with frequencies less than 30 cm^{-1}, the normal mode analysis is significant, because it defines a natural and useful set of collective variables to describe such motions. In a paper for the result of analysis of the Monte Carlo simula-

tion,[25] anharmonic aspects of conformational dynamics corresponding to the existence of multiple minima will be discussed, which will enrich the dynamic picture developed in this paper based on the normal mode analysis.

ACKNOWLEDGMENTS

We thank Dr. T. Noguti for helpful discussions and Mr. J. Higo for preparation of some of the figures in this report. Computations were done at Computer Centers of Kyushu University and of the Institute for Molecular Science. This work was supported by grants from MESC and STA.

REFERENCES

1. McCammon, J.A., Karplus, M. Simulation of protein dynamics. Annu. Rev. Phys. Chem. 31:29–45, 1980.
2. Karplus, M., McCammon, J.A. The internal dynamics of globular proteins. CRC Crit. Rev. Biochem. 9:293–349, 1981.
3. Levitt, M. Protein conformation, dynamics and folding by computer simulation. Annu. Rev. Biophys. Bioeng. 11:251–271, 1982.
4. Karplus, M., McCammon, J.A. Dynamics of proteins: Elements and function. Annu. Rev. Biochem. 53:263–300, 1983.
5. Levy, R.M., Keepers, J.W. Computer simulation of protein dynamics: Theory and experiment. Comments Mol. Cel. Biophys. 3:273–294, 1986.
6. Gō, N., Noguti, T., Nishikawa, T. Dynamics of a small protein in terms of low-frequency vibrational modes. Proc. Natl. Acad. Sci. U.S.A. 80:3696–3700, 1983.
7. Brooks, B., Karplus, M. Harmonic dynamics of proteins: Normal modes and fluctuations in bovine pancreatic trypsin inhibitor. Proc. Natl. Acad. Sci. U.S.A. 80:6571–6575, 1983.
8. Levitt, M., Sander, C., Stern, P.S.. The normal modes of a protein: Native bovine pancreatic trypsin inhibitor. Int. J. Quant. Chem.: Quant. Biol. Symp. 10:181–199, 1983.
9. Levitt, M., Sander, C., Stern, P.S. Protein normal-mode dynamics: Trypsin inhibitor, crambin, ribonuclease and lysozyme. J. Mol. Biol. 181:423–447, 1985.
10. Noguti, T., Gō, N. Collective variable description of small-amplitude conformational fluctuations in a globular protein. Nature 296:776–778, 1982.
11. Huber, R., Bennett, W.S. Functional significance of flexibility in proteins. Biopolymers 22:261–279, 1983.
12. Noguti, T., Gō, N. Efficient Monte Carlo method for simulation of fluctuating conformations of native proteins. Biopolymers 24:527–546, 1985.
13. Braun, W., Gō, N. Calculation of protein conformations by proton-proton distance constraints: A new algorithm. J. Mol. Biol. 186:611–626, 1985.
14. Marquart, M., Walter, J., Deisenhofer, J., Bode, W., Huber, R. The geometry of the reactive site and of the peptide groups in trypsin, trypsinogen and its complexes with inhibitors. Acta Cryst. Sect B. 39:480–490, 1983.
15. Deisenhofer, J., Steigemann, W. Crystallographic refinement of the structure of bovine pancreatic trypsin inhibitor at 1.5 Å resolution. Acta Cryst. Sect B. 31:238–250, 1975.
16. Dunfield, L., Burgess, A.W., Scheraga, H.A. Energy parameters in polypeptides. 8. Empirical potential energy algorithm for the conformational analysis of large molecules. J. Phys. Chem. 82:2609–2616, 1978.
17. Noguti, T., Gō, N. A method of rapid calculation of a second derivative matrix of conformational energy for large molecules. J. Phys. Soc. Japan 52:3685–3690, 1983.
18. Abe, H., Braun, W., Noguti, T., Gō, N. Rapid calculation of first and second derivatives of conformational energy with respect to dihedral angles for proteins. General recurrent equations. Computers Chem. 8:239–247, 1984.
19. Wilson, E.B., Decius, J.C., Cross, P.C. In "Molecular Vibrations." New York: McGraw-Hill. 1955:11–33.
20. Eckart, C. Some studies concerning rotating axes and polyatomic molecules. Phys. Rev. 47:552–558, 1935.
21. Noguti, T., Gō, N. Dynamics of native globular proteins in terms of dihedral angles. J. Phys. Soc. Jpn. 52:3283–3288, 1983.
22. Swaminathan, S., Ichiye, T., Gunsteren, W.V., Karplus, M. Time dependence of atomic fluctuations in proteins: Analysis of local and collective motions in bovine pancreatic trypsin inhibitor. Biochemistry 21:5230–5241, 1982.
23. Suezaki, Y., Gō, N. Fluctuations and mechanical strength of α-helices of polyglycine and poly(L-alanine). Biopolymers 15:2137–2153, 1976.
24. Tawada, K., Kimura, M. Stiffness of carbodiimide-cross-linked glycerinated muscle fibers in rigor and relaxing solutions at high salt concentrations. J. Muscle Res. Cell Motil. 7:339–350, 1986.
25. Noguti, T., Gō, N. In preparation.